PAPER

Check for updates

Enhancing capacitance of supercapacitor with both organic electrolyte and ionic liquid electrolyte on a biomass-derived carbon†

Xuehang Wang,‡[a] Yahao Li,‡[a] Fengliu Lou,[a] Marthe Emelie Melandsø Buan,[a] Edel Sheridan[b] and De Chen [iD] *[a]

Supercapacitor (SC) with organic electrolyte or ionic liquid (IL) electrolyte can generally store/release higher energy than that with an aqueous electrolyte, due to a larger operating voltage window of a non-aqueous electrolytes. A carbon is synthesized by a facile impregnate-activation method from renewable woody biomass, which has twice of the specific surface area and pore volume than the sample synthesized by conventional KOH activation. Biomass-derived carbons with high ion accessible surface area and highly integrated micropores and mesopores provide superior capacitance, excellent rate capability and good stability in both organic electrolyte and IL electrolytes. Significant enhancement in the capacitance and rate capability were obtained by the generation of micropores similar to the ion size and better pore network through removal of impurities in the biomass. High specific capacitances of 146 F g^{-1} in the organic electrolyte and 224 F g^{-1} in the IL electrolyte at current density of 0.1 A g^{-1} are achieved. Highly integrated micro- and mesoporous structure leads to a good rate capability of 100% capacitance retention at current density up to 10 A g^{-1} in the organic electrolyte and 67% capacitance retention at current density up to 7 A g^{-1} in the IL. With the large voltage offered by the non-aqueous electrolyte, the material can store/release high maximum energy of 26 W h kg^{-1} and 92 W h kg^{-1} in the organic electrolyte and IL electrolyte, respectively. It reveals that the biomass derived carbon is a promising and cost effective candidate for electrodes in high performance SCs.

Introduction

Supercapacitors (SCs, also known as electrochemical capacitors) are promising energy storage devices to replace the batteries for mobile power supply applications, which demand short charge/discharge rate, high power, long cycling life, low cost, reliability and safety.[1] Commercially available SCs using porous activated carbon (AC) as the electrode active material can deliver a specific capacitance of 80–120 F g^{-1} and a packaged full-cell energy density of 4–5 W h kg^{-1}.[2] Meanwhile, the typical energy for lead acid battery and nickel–cadmium battery is 25–35 W h kg^{-1} and 40–60 W h kg^{-1}, respectively.[3] The relatively low energy density of the commercial SCs is a fatal drawback that renders SCs compensation to the batteries, instead of replacement, in the mobile energy storage applications.

[a]*Department of Chemical Engineering, Norwegian University of Science and Technology, Sem Sælands vei 4, 7491 Trondheim, Norway. E-mail: de.chen@ntnu. no; Fax: +47 735 95047; Tel: +47 735 93149*

[b]*SINTEF Materials and Chemistry, 7491 Trondheim, Norway*

† Electronic supplementary information (ESI) available. See DOI: 10.1039/c7ra01630a

‡ Authors attribute equally to this paper.

As the energy density (E) of a SC is determined by: $E = 1/2CV^2$, either increasing the specific capacitance (C) or the operating voltage window (V) increases the energy of SCs.[4,5] The highest specific capacitance was reported to be up to 800 F g^{-1} in an H$_2$SO$_4$ aqueous electrolyte.[6] However, the energy of SCs using the aqueous solution as electrolyte is generally lower than that in the non-aqueous electrolyte, as the operating voltage is generally <1 V for the aqueous solution, but 2–3 V for the organic electrolyte and 3–5 V for the neat ionic liquid (IL). To achieve similar energy of the best double layer SC with aqueous solution (∼1000 F g^{-1}), capacitance of 128 F g^{-1} (organic electrolyte) and 65 F g^{-1} (IL) are required, which have already been reached in many reported materials.[5,7–9] Thus, the rising of the capacitance in the non-aqueous electrolyte, especially in the neat IL, is efficient to improve the energy of SCs.

Specific surface area (SSA) has been considered as the key factor to specific capacitance as the SSA was found to have a linear relationship with the specific capacitance based on $C = \varepsilon_0\varepsilon_r A/d$. It is not necessary the case when the SSA is very large (>2000 m^2 g^{-1}).[10] The largest SSA reported in literature is limited at 4000 m^2 g^{-1},[11] but the material shows a relatively low normalize capacitance (capacitance normalized by surface area) with a moderate specific capacitance of 165 F g^{-1} with aqueous electrolyte. The normalized capacitance was found to be related

with pore sizes. Despite the use of organic electrolyte or IL, the pore with pore size close to the ion size delivers the highest normalized capacitance.[12,13] For the typical organic electrolyte, the optimized pore size is 0.7–0.8 nm,[12] whereas the optimized pore size for typical IL is 0.9–1.3 nm.[14] In mesoporous region, there is another pore size distribution (PSD) region, also offers enhanced normalized capacitance for the IL electrolyte.[14]

The hard and soft template methods are used to synthesis mesoporous carbon with well-controlled pore size. However, the method is complicated and the maximum specific capacitance of the resulting material is limited due to the moderate specific surface area compared to that of the ACs.[15–17] Activation treatment is also an efficient way to generate micro- and mesopores with tunable average pore size and large SSA. Synthetic polymers,[18–20] natural materials,[21,22] carbon nanofibers, carbon nanotubes[23,24] and graphene[25] have all been used as the activation precursor. In our previous work, we reported a polymer-derived mesopores-rich carbon which showed a high specific capacitance of 290 F g^{-1} in IL electrolyte.[14,19] Unlike the synthetic polymer or other synthetic carbon material, it is facile and cost effective to use the renewable nature resources, woody biomass, as the activation precursors.[26–28] The major drawback of using the biomass precursor is the reproducibility among each production batch. Pine tree sawdust powder, a woody biomass, is a common waste in the lumberyards and woodworking shops around the world. The activated pine tree powder has been used for waste removal from the aqueous solution[29,30] and electrode material of the SC.[26] In this work, we explore a facile method for synthesis and treatment of highly porous carbon with rich mesopores from pine tree powder, as cost effective and high performance electrodes in SCs. The pore size and distribution are manipulated to achieve superior capacitive performance, excellent rate capability and good stability in both tetraethylammonium tetrafluoroborate/acetonitrile (TEABF$_4$/AN) organic electrolyte and the 1-ethyl-3-methylimidazolium tetrafluoroborate (EMIMBF$_4$) IL electrolyte. Higher capacitance and specific energy will be reported compared to the conventional active carbons. Moreover, by comparing the capacitive performance of the organic and the IL electrolyte, the relationship between the texture properties and performance for both electrolytes is revealed.

Results and discussion

A highly porous carbon with BET surface area of 2207 m^2 g^{-1}, namely APN-IMPREG-HCl, was synthesized by impregnate-activation method of a pine tree sawdust powder, followed by a HCl reflux washing step (route 1 in Fig. 1a). Scanning electron microscopy (SEM) image showed an irregular particle structure of the APN-IMPREG-HCl at low magnification (Fig. 1b) and a porous surface at high magnification (Fig. 1b inset). Typical KOH activation is also applied to the pine tree sawdust powder, the resulting material was marked as APN-KOH (route 2). The Brunauer–Emmett–Teller (BET) surface area and the total pore volume (>0.9 nm) of the APN-KOH are 1018 m^2 g^{-1} and 0.60 cm^3 g^{-1}, respectively. The BET surface area, as well as the nanopores volume almost doubled after the activation method changed

into the impregnate-activation method. Before the HCl reflux (sample named as APN-IMPREG), the sample showed a mesopores-rich structure as 74% of the pore volume was contributed by the mesopores with pore size >2 nm. After the HCl reflux, the BET surface area increased insignificantly from 2029 m^2 g^{-1} to 2207 m^2 g^{-1} and the total pores volume also slightly increased from 1.34 cm^3 g^{-1} to 1.41 cm^3 g^{-1}. The N$_2$ isotherm of these three materials all belong to type IV (Fig. 1c), with negligible hysteresis and small N$_2$ uptake as the relative pressure is greater than 0.4. That indicates that the pores in the material are mostly micropores and small mesopores.[31,32] Comparing the structure of PSD between the APN-IMPREG and APN-IMPREG-HCl (Fig. 1d), the PSD in mesoporous regions are similar with each other, whereas the APN-IMPREG-HCl has more pores distributed in the microporous region (0.9–2 nm). The HCl reflux increased micropores volume from 0.29 to 0.31 cm^3 g^{-1}, but did not change the mesopores volume. The pore structure could vary among batches as the precursor is a biomass.

The X-ray photoelectron spectroscopy (XPS) spectra show both the APN-IMPREG and the APN-IMPREG-HCl is dominated by C, O and N species (Fig. 1e). Besides the presence of F, P and B species, a few Fe and Al species are also observed in the APN-IMPREG material. The Al and Fe species were totally removed after the HCl reflux, which can explain the PSD difference before and after HCl reflux. The APN-IMPREG-HCl has more micropores than the APN-IMPREG, which may be related to the removal of the metal species in the micropores.

The performances of the SCs using the APN-IMPREG, APN-IMPREG-HCl and APN-KOH as the active electrode material were tested in two-electrode symmetric coin cells. Non-aqueous electrolytes, including organic solution and IL, were used as the electrolyte of SCs. The performance of the APN-IMPREG and the APN-IMPREG-HCl using the 1 M TEABF$_4$/AN organic electrolyte are compared with those of the APN-KOH in Fig. 2a–c. We observed the capacitive properties of the carbon material activated from pine tree sawdust powder based on the triangular shape of the charge/discharge curves. Three material all showed high current efficiency (above 95%) at the current density of 1 A g^{-1} (Fig. 2a), indicating efficient cycling ability at the current density of 1 A g^{-1}. The capacitance, calculated based on the discharge time on the charge/discharge curve, increases in the sequence of APN-KOH, APN-IMPREG and APN-IMPREG-HCl. The capacitance of the APN-IMPREG-HCl in the organic electrolyte is 146 F g^{-1} at the current density of 1 A g^{-1}. The capacitance shows no down trend up to 10 A g^{-1}, demonstrating a very good rate capability the material with organic electrolyte. As shown in Fig. 2c, the nearly perfect rectangular-shaped loop is obtained at sweep rates from 50 mV s^{-1} to 500 mV s^{-1} without any redox peaks, further supporting the good capacitive behavior and rate capability of the APN-IMPREG-HCl. In the organic electrolyte, three carbon materials all show good rate capability and similar voltage drop as the current densities increase from 1 to 10 A g^{-1} (Fig. 2b). The rate capability derived from the CV analyses (Fig. 2c inset) shows worse rate capability of 77% of the capacitance retention at scan rate of 500 mV s^{-1}. Detailed capacitance changes with the current density or the scan rate are given in detail as Table S1.†
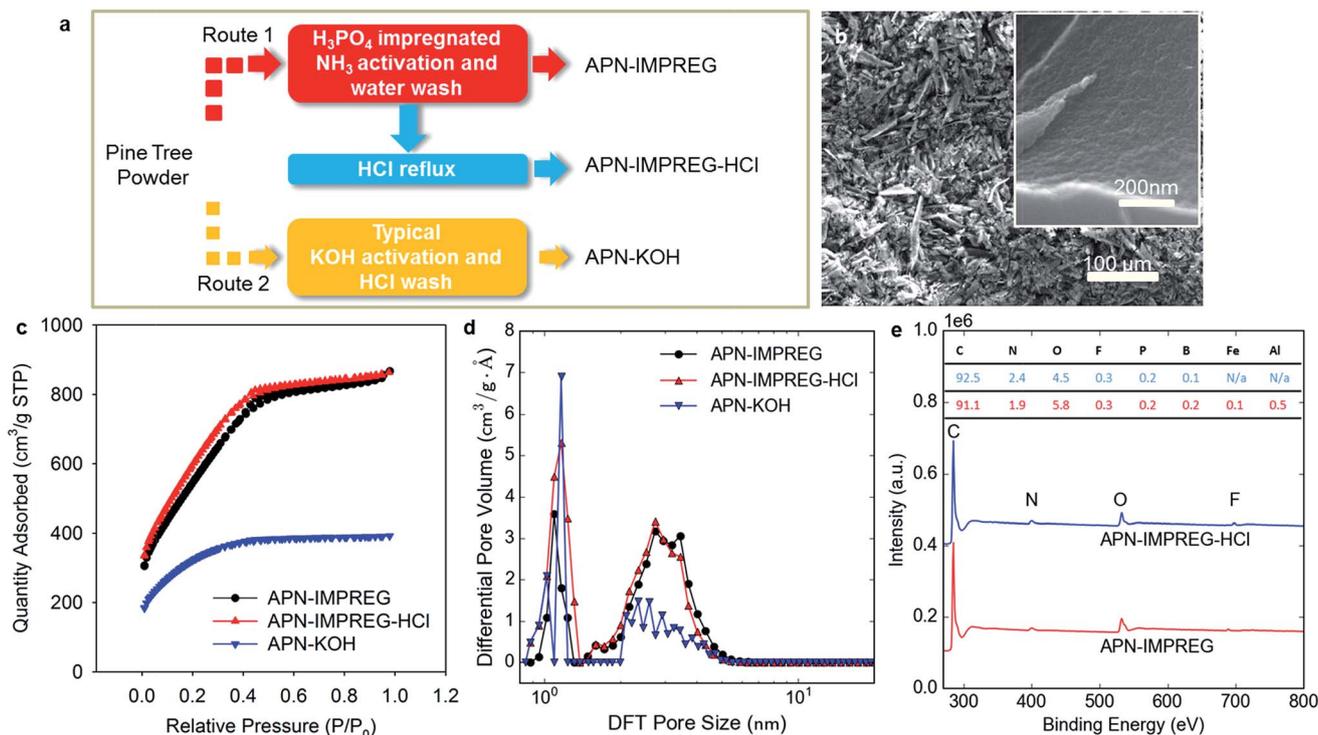
Fig. 1 (a) Schematic of synthesizing step, (b) SEM image of APN–IMPREG–HCl with low and high (inset) magnification, (c) N_2 isotherm, (d) PSD curve derived by 2D NLDFT method, (e) XPS spectra and inset is a table of detailed elements in materials.

When the IL is used as the electrolyte, the SC using three carbon materials still displayed good capacitive behavior (Fig. 2d). The capacitances were calculated to be 140 F g^{-1}, 184 F g^{-1} and 131 F g^{-1} for the APN-IMPREG, APN-IMPREG-HCl and APN-KOH, respectively, at current density of 1 A g^{-1}. Among these three samples, the APN-IMPREG-HCl not only showed the highest capacitance of 224 F g^{-1} at 0.1 A g^{-1}, but also the best capacitance retention of 67% at current density up to 7 A g^{-1}. The CV curve of the APN-IMPREG-HCl in the IL also showed a good rectangular shape up to 300 mV s^{-1} (Fig. 2f). The capacitance retention at the scan rate of 500 mV s^{-1} based on the CV curve is 57% compared to the capacitance tested at 50 mV s^{-1} (Fig. 2f inset). Although the APN-IMPREG-HCl has more micropores than the APN-IMPREG, the APN-IMPREG-HCl still showed better rate capability and lower voltage drop. That is probably due to the absence of the metal impurities in the APN-IMPREG-HCl.

Due to the larger ion transportation resistance of the IL than that of the organic electrolyte with solvent, worse rate capability and higher voltage drop are expected in the IL than in the organic electrolyte (Fig. 2e and f inset). In general, the voltage drop with the IL electrolyte is larger than that with the organic electrolyte. That is due to the low conductivity and large viscosity of IL compared to organic electrolyte.[33] For IL electrolyte, the APN-IMPREG-HCl showed a voltage drop of 0.15 V at the current density of 1 A g^{-1} and a voltage drop of 0.7 V at the current density of 7 A g^{-1}. The voltage drop of APN-IMPREG-HCl with IL electrolyte is much lower compared to the other two materials in this work. Thus, the APN-IMPREG-HCl showed its

privileged performance with high capacitance and good rate capability in both the organic electrolyte and the IL electrolyte in this work.

The highest normalized capacitance is reached when the pore size matches the ion size, and TEA$^+$ in organic electrolyte is 0.68 nm in size. The formation of the solvation shell in the organic electrolyte makes the pores with pore size around 1–2 nm the lowest normalized capacitance.[12] That means the pores with pore size of 1–2 nm does not efficiently contribute to the capacitance in organic electrolyte. However, the pores with pore size of 0.9–1.3 nm has the highest normalized capacitance for the IL EMIMBF$_4$ electrolyte.[14] Interestingly, the ratio of the experimental capacitance with IL electrolyte over organic electrolyte (C_{IL}/C_{org}) increases as the ratio between micropores volume (0.9–2 nm) and total pore volume increases (Table 1). That indicates micropores with pore size between 0.9 to 2 nm has more effect on the capacitance with the IL electrolyte rather than with the organic electrolyte, which is in consistent with the reported pore size effect on the capacitance.[12,13]

The specific surface area and the PSD are two key parameters to the double layer capacitance of SCs. Pine tree sawdust powder activated by the conventional KOH activation (APN-KOH) has a relatively low specific surface area of 1018 m^2 g^{-1}. Introducing a more severe condition by impregnating the material with acid and activating the impregnated material in a basic atmosphere, effectively improved the resulting specific surface area and the total pore volume after activation (Table S2†). The specific surface area of the APN-IMPREG is around two times of the
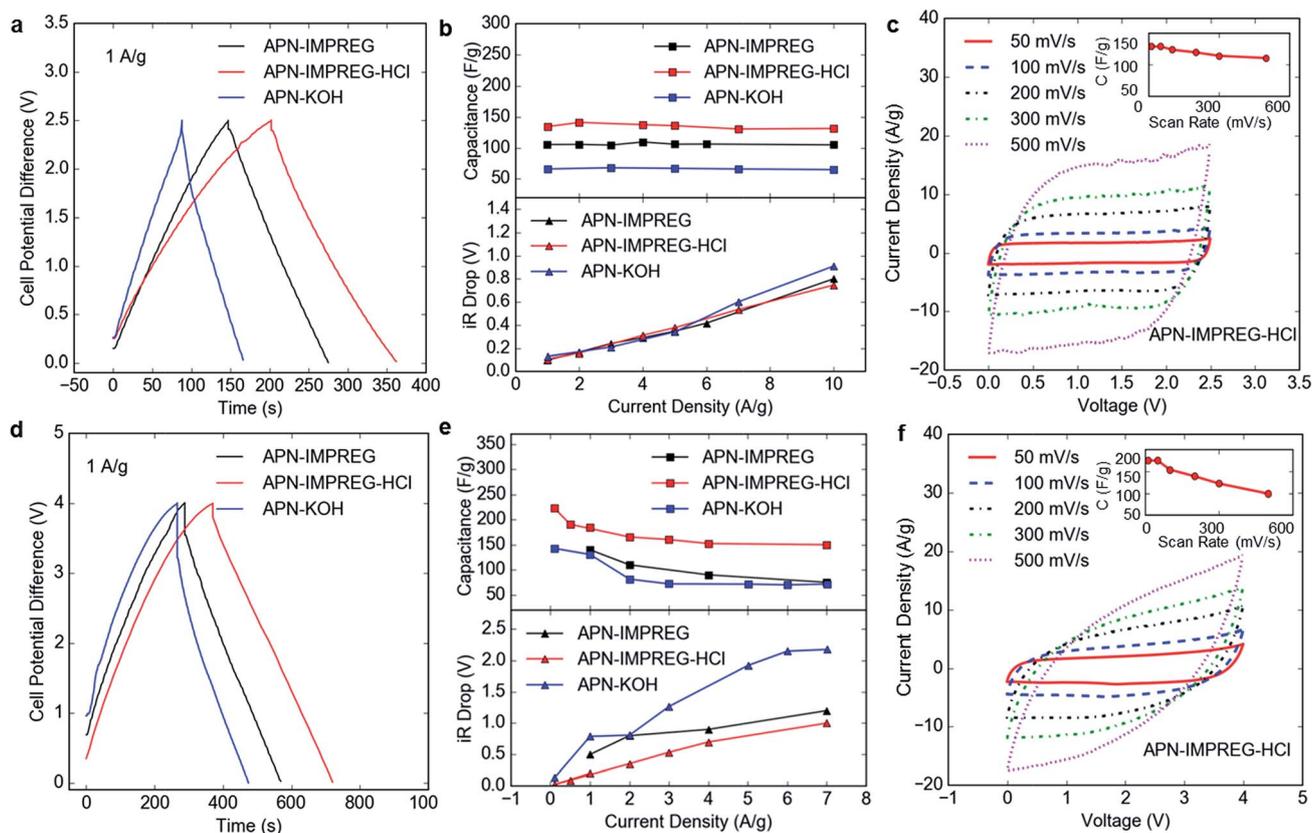
Fig. 2 Organic electrolyte: (a) charge/discharge curve, (b) capacitance and voltage drop change with current density, (c) CV curve, inset is capacitance *vs.* scan rate; neat IL: (d) charge/discharge curve, (e) capacitance and voltage drop change with current density, (f) CV curve, inset is capacitance *vs.* scan rate.

value of APN-KOH and the mesopores volume with pore size > 2 nm also increases from 0.28 to 0.98 cm^3 g^{-1}. The capacitance of APN-IMPREG is 37% higher than the APN-KOH for organic electrolyte, whereas only 8% for IL electrolyte (Table S2†). As the micropores of the material has more impact on the capacitance with the IL electrolyte (rather than the organic electrolyte), the relative insignificant improvement of the capacitance with the IL electrolyte seems to suggest the micropores volume that can be penetrated by the IL is not as high as that can be accessed by N$_2$. That could be related to the partial blocking of the micropores by the impurities.

By the HCl reflux, metal species in the precursor were removed and some totally blocked micropores (pores cannot be penetrated by N$_2$) are opened, leading to only 5% of increase in the pore volume. The capacitance, however, has an increase of 27% with the organic electrolyte and 24% with the IL electrolyte (Table S2†). Notably, the mesopores volume of APN-IMPREG-HCl is almost the same as the APN-IMPREG, whereas the micropores volume increases 17%. The increase in the capacitance could relate to the micropores (0.9–1.3 nm) opening by impurities removal. The significant capacitance increase with micropores volume increase agrees well with that the pore with the size similar to the ion size provides ultrahigh normalized capacitance.[12–14] However, the increase in the capacitance cannot be only assigned to the micropores volume changes validated by the N$_2$ isotherm test, as the enhancement of the capacitance was more significant than the improvement of micropores volume.

Table 1 Pore characteristics and capacitance comparison between organic electrolyte and IL electrolyte

Sample	Total pore volume (0.9 nm to ~60 nm) (cm^3 g^{-1})	Specific surface area (m^2 g^{-1})	Micropores volume (pore size 0.9–2 nm)	Mesopores volume (2 nm to ~60 nm)	Micropore volume/ total pore volume (cm^3 g^{-1})	$C_{\text{IL}}/C_{\text{org}}$
APN-IMPREG	1.34	2029	0.36	0.98	0.26	1.33
APN-IMPREG-HCl	1.41	2207	0.42	0.99	0.31	1.37
APN-KOH	0.60	1018	0.32	0.28	0.53	1.68
Pollen-derived carbon[34]	2.27	3037	0.41	1.86	0.18	1.11

Based on an ion packing model (model deviation is described in detail in ESI† and ref. 14), the capacitance of the material with IL can be estimated by the pore size distribution itself.[14] Using the pore size distribution of the APN-IMPREG and APN-IMPREG-HCl, the capacitance is estimated to be 160 F g^{-1} and 185 F g^{-1}, respectively. The estimated value agrees well with the experimental result of APN-IMPREG-HCl, but is higher than the experimental result of APN-IMPREG. That can be explained that there are a large number of micropores and mesopores (>0.9 nm) in the APN-IMPREG that can be accessed by N_2 but cannot be accessed by the ions in the electrolyte before HCl reflux. That means some micro- and mesopores are partially blocked, and cannot contribute to the total capacitance. Thus, the HCl reflux process not only opens the micropores that are totally blocked (Fig. 1a), but also removes the impurities that hinders the transportation of the ions inside the micro- and mesopores.

The electrochemical impedance spectroscopy (EIS) measurements are performed to analyze the SCs using the APN-IMPREG and APN-IMPREG-HCl. As shown in Fig. 3a and b, the near vertical curve in the low frequency region of both the organic electrolyte and the IL electrolyte indicates the capacitive behavior of SCs. In the higher frequency region of Nyquist plot for organic electrolyte, the sample before and after HCl reflux showed similar equivalent series resistances (ESRs). The ion diffusion resistance is reflected by the Warburg region with a slope of 45° portion on the Nyquist curve (red dash line marked 45° angle). The APN-IMPREG-HCl showed larger ion diffusion resistance than the APN-IMPREG.

For IL electrolyte, the Warburg region for APN-IMPREG-HCl and APN-IMPREG are similar. However, the ESR of the APN-IMPREG-HCl is much larger than that of the APN-IMPREG. The intrinsic electronic properties of the active electrode material and the electrolyte, mass transfer resistance of the ions in the pores, as well as the contact resistance between the active electrode material and the current collector all contribute to the ESR arising.[1] Thus, the APN-IMPREG-HCl has a higher mass transfer resistance than the APN-IMPREG with both the organic electrolyte and IL electrolyte. The increased apparent mass transfer resistance measured by impedance spectroscopy is most likely because the ions in APN-IMPREG-HCl can access more micro-/mesopores and transport deeper into the pores
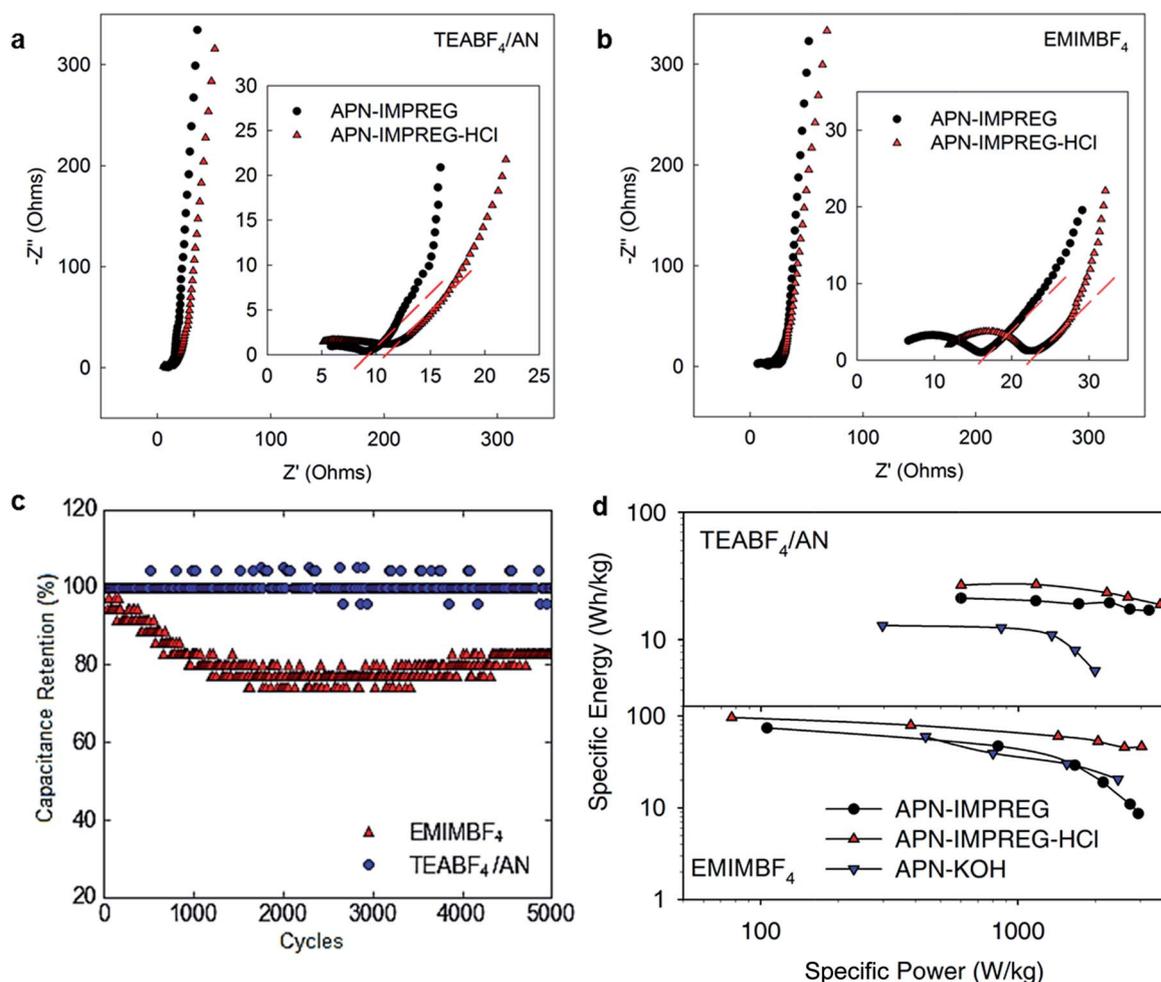

Fig. 3 (a) Nyquist plot with organic electrolyte, (b) Nyquist plot with IL electrolyte, (c) cycling stability of APN–IMPREG–HCl with organic and IL electrolyte, (d) Ragone plot of SC with organic electrolyte and IL electrolyte.

than APN-IMPREG. That further support the removal of the impurities offers more micro- and mesopores accessible for the ions, and leads to higher capacitance.

The cycling stability of the APN-IMPREG-HCl was tested under the current density of 5 A g^{-1}, the capacitance in the organic electrolyte showed almost no loss after 5000 cycles. The capacitance retention of the APN-IMPREG-HCl is also relatively good with 80% retention after 5000 cycles, indicating the material can be used in a high voltage of 4 V.

The energy density of the material was further calculated based on $E = 1/2CV^2$. Here, C is the capacitance of the total cell ($C_{total} = 0.25$ single electrode capacitance) and V is the cell's potential difference (exclude the iR drop). The AC derived from coconut shell, which is the active electrode material used in the commercial SC, has a specific surface area of ~1500 m^2 g^{-1} and capacitance of 80–120 F g^{-1} with conventional organic electrolyte of 1 M TEABF$_4$/AN. Comparing to the conventional SC using coconut shell derived AC, the impregnated-activated porous carbon APN-IMPREG-HCl shows a high capacitance in organic electrolyte. As discussed above, as the PSD of the APN-IMPREG-HCl is more efficiently used by the IL electrolyte and IL offers a large operating voltage window, a specific energy of 92 W h kg^{-1} was achieved of the SC using the IL as electrolyte, which is higher than the reported values for biomass derived carbon-IL system. The Ragone plot showing the relationship between the specific energy and the specific power also shows that the APN-IMPREG-HCl delivered the best performance within the pine tree derived carbon reported in this work (Fig. 3d). Furthermore, the capacitance and the energy of the active materials in this work are also compared with other reported biomass-derived carbon in Table S2.† Although, the APN-IMPREG-HCl showed relatively worse performance than that of the pollen derived carbon,[34] the cheap price and large production of the pine tree dust powder still showed the advantage of using the pine tree dust powder derived carbon.

Experimental

Synthesis of the pine tree powder derived carbon

Two activation methods are applied to the pine tree sawdust powder (grinded with particle size of <75 μm) as shown in Fig. 1a, namely conventional KOH activation and impregnate-activation. For the KOH activation, the pine tree sawdust power was milled with KOH plates with the mass ratio of 1 : 4 before heating up (activation) under the Ar flow of 100 mL min^{-1}. The maximum activation temperature is 850 °C with a heating rate of 10 °C min and 1 hour dwell. Afterwards, the sample (namely APN-KOH) was washed by HCl in order to remove the accessed K species. For impregnate-activation, a porous carbon was produced by firstly impregnating the pine tree powder by 1.5 M H$_3$PO$_4$ solution (1 g solid: 50 mL solution) and then activated by NH$_3$ gas flow (50 mL min^{-1}) in the tube furnace. Before activation, the sample was dried overnight to remove the excess water. During activation, the sample was heated up to 1000 °C with a heating rate of 5 °C min before the maximum temperature was kept for 2 hours. The sample was then refluxed by distilled water over night and named as

APN-IMPREG. Moreover, the APN-IMPREG was refluxed by excessive 1 M HCl solution overnight, washed several times by distilled water until the pH became 7 and marked as APN-IMPREG-HCl. The yield from the pine tree sawdust powder to the APN-IMPREG-HCl is around 10%.

Material characterization

SEM analysis was carried out on a Hitachi S-5500 S(T)EM instrument. The nitrogen sorption (−196 °C) isotherms were performed on a Micromeritics Tristar II 3020 instrument to obtain the BET surface area and the PSD of the materials (relative pressure range from 0.001 to 1). 2D NLDFT method was applied to get the PSD based the N$_2$ isotherm.[35,36] Before the isothermal test, each sample was degassed at 200 °C for 12 hours under turbomolecular vacuum pumping. XPS measurements were carried using a Kratos Axis Ultra DLD spectrometer with a monochromatic AlKα radiation ($hv = 1486.6$ eV).

Electrochemical measurements

The prepared carbon powders were milled with 5 wt% polytetrafluoroethylene (PTFE aqueous solution, Sigma-Aldrich) in a small amount of ethanol. The carbon–PTFE mixtures were used to fabricate SC electrodes by pressing the mixtures over a nickel foam disk (Alfa Aesar) at 6 MPa for two minutes. The mass loading of the active material was approximately 2 mg cm^{-2}. The electrodes were dried in vacuum oven at 120 °C for 12 hours before assembling.

Electrochemical tests in this study were conducted in a two-electrode cell configuration using 2016 coin cells. The assembling of all components of the cell are carried out in an argon filled glovebox. Two electrodes with the same loading were separated by a 25 μm thin microporous monolayer membrane (Celgard 3501) separator. 15 μL of neat IL EMIMBF$_4$ (Sigma-Aldrich) or 1 M TEABF$_4$/acetonitrile (Sigma-Aldrich) was added to each side of the separator as electrolyte of the SCs. The prepared SCs were stabilized overnight before performance tests.

Conclusions

Here we report the carbons produced from renewable woody biomass by a facile method as cost effective electrode materials in the both organic electrolyte and IL electrolyte. The facile method using impregnate-activation procedure followed by a HCl reflux resulted in a doubled specific surface area and three times of mesoporous volume compared to the sample activated by the conventional KOH activation. For all the carbon materials, the IL electrolyte resulted in not only the higher operating voltage window but also higher capacitance, thus much higher energy density compared to the organic electrolyte. Although the ion size of EMIM$^+$ in IL is larger than the one of TEA$^+$ in organic electrolyte, the solvation shell of the TEA$^+$ reduces its access to micropores. The impurities removal by HCl reflux generated the micropores with the size close to 1 nm. Such pores with similar size of ions in the electrolyte significantly enhanced the storage of ions in these confined pore

volumes, thus drastically increased the capacitance in IL electrolyte-carbon system. The impurities removal also opens the partial blocked micro- and mesopores to further enhance the capacitance. Hierarchical pore structure with highly integrated micro- and mesopores also results in a superior rate capability of the material in both organic and IL electrolyte.

The resulted renewable carbon electrodes exhibit superior capacitive performance, including high specific capacitance, impressive rate performance, and excellent cycle stability. High specific capacitances of 146 F g^{-1} in the organic electrolyte and 224 F g^{-1} in the IL electrolyte at the current density of 0.1 A g^{-1} are achieved. Highly integrated micro- and mesoporous structure leads to a good rate capability of 100% capacitance retention at current density up to 10 A g^{-1} in the organic electrolyte and 67% capacitance retention at current density up to 7 A g^{-1} in the IL. With the large voltage offered by the non-aqueous electrolyte, the material can store/release high maximum energy of 26 W h kg^{-1} and 92 W h kg^{-1} in the organic electrolyte and IL electrolyte, respectively. Due to high abundance, low cost, and high performance, carbon from pine woody biomass is an excellent candidate for the electrodes of SCs.

Acknowledgements

Notes and references

1 Y. Li, Z. Li and P. K. Shen, *Adv. Mater.*, 2013, **25**, 2474–2480.
2 A. Burke, *Electrochim. Acta*, 2007, **53**, 1083–1091.
3 D. Linden and T. B. Reddy, *Handbook of Batteries, McGraw-Hill*, New York, USA, 3rd edn, 2002.
4 F. Béguin, V. Presser, A. Balducci and E. Frackowiak, *Adv. Mater.*, 2014, **26**, 2219–2251.
5 G. Wang, L. Zhang and J. Zhang, *Chem. Soc. Rev.*, 2012, **41**, 797–828.
6 T. Lin, I.-W. Chen, F. Liu, C. Yang, H. Bi, F. Xu and F. Huang, *Science*, 2015, **350**, 1508–1513.
7 S. Faraji and F. N. Ani, *Renewable Sustainable Energy Rev.*, 2015, **42**, 823–834.
8 L. L. Zhang and X. Zhao, *Chem. Soc. Rev.*, 2009, **38**, 2520–2531.
9 C. Liu, Z. Yu, D. Neff, A. Zhamu and B. Z. Jang, *Nano Lett.*, 2010, **10**, 4863–4868.
10 M. Lu, F. Beguin and E. Frackowiak, *Supercapacitors: materials, systems and applications*, John Wiley & Sons, 2013.
11 J. W. To, Z. Chen, H. Yao, J. He, K. Kim, H.-H. Chou, L. Pan, J. Wilcox, Y. Cui and Z. Bao, *ACS Cent. Sci.*, 2015, **1**, 68–76.
12 J. Chmiola, G. Yushin, Y. Gogotsi, C. Portet, P. Simon and P.-L. Taberna, *Science*, 2006, **313**, 1760–1763.
13 C. Largeot, C. Portet, J. Chmiola, P.-L. Taberna, Y. Gogotsi and P. Simon, *J. Am. Chem. Soc.*, 2008, **130**, 2730–2731.
14 X. Wang, H. Zhou, E. Sheridan, J. C. Walmsley, D. Ren and D. Chen, *Energy Environ. Sci.*, 2016, **9**, 232–239.
15 H.-Q. Li, R.-L. Liu, D.-Y. Zhao and Y.-Y. Xia, *Carbon*, 2007, **45**, 2628–2635.
16 Y. Korenblit, M. Rose, E. Kockrick, L. Borchardt, A. Kvit, S. Kaskel and G. Yushin, *ACS Nano*, 2010, **4**, 1337–1344.
17 A. Kajdos, A. Kvit, F. Jones, J. Jagiello and G. Yushin, *J. Am. Chem. Soc.*, 2010, **132**, 3252–3253.
18 B. Xu, F. Wu, S. Chen, C. Zhang, G. Cao and Y. Yang, *Electrochim. Acta*, 2007, **52**, 4595–4598.
19 X. Wang, H. Zhou, F. Lou, Y. Li, M. E. Buan, X. Duan, J. C. Walmsley, E. Sheridan and D. Chen, *ChemSusChem*, 2016, **9**, 3093–3101.
20 B. Xu, S. Hou, G. Cao, M. Chu and Y. Yang, *RSC Adv.*, 2013, **3**, 17500–17506.
21 J. I. Hayashi, A. Kazehaya, K. Muroyama and A. P. Watkinson, *Carbon*, 2000, **38**, 1873–1878.
22 H. Wang, S. Yu and B. Xu, *Chem. Commun.*, 2016, **52**, 11512–11515.
23 E. Raymundo-Pinero, P. Azais, T. Cacciaguerra, D. Cazorla-Amorós, A. Linares-Solano and F. Béguin, *Carbon*, 2005, **43**, 786–795.
24 V. Barranco, M. Lillo-Rodenas, A. Linares-Solano, A. Oya, F. Pico, J. Ibañez, F. Agullo-Rueda, J. Amarilla and J. Rojo, *J. Phys. Chem. C*, 2010, **114**, 10302–10307.
25 Y. Zhu, S. Murali, M. D. Stoller, K. Ganesh, W. Cai, P. J. Ferreira, A. Pirkle, R. M. Wallace, K. A. Cychosz and M. Thommes, *Science*, 2011, **332**, 1537–1541.
26 N. Manyala, A. Bello, F. Barzegar, A. A. Khaleed, D. Y. Momodu and J. K. Dangbegnon, *Mater. Chem. Phys.*, 2016, **182**, 139–147.
27 D. Momodu, M. Madito, F. Barzegar, A. Bello, A. Khaleed, O. Olaniyan, J. Dangbegnon and N. Manyala, *J. Solid State Electrochem.*, 2016, 1–14.
28 A. Cuña, N. Tancredi, J. Bussi, V. Barranco, T. A. Centeno, A. Quevedo and J. M. Rojo, *J. Electrochem. Soc.*, 2014, **161**, A1806–A1811.
29 P. Nowicki and R. Pietrzak, *Bioresour. Technol.*, 2010, **101**, 5802–5807.
30 M. C. Tonucci, L. V. A. Gurgel and S. F. de Aquino, *Ind. Crops Prod.*, 2015, **74**, 111–121.
31 Z. Ryu, J. Zheng, M. Wang and B. Zhang, *Carbon*, 1999, **37**, 1257–1264.
32 M. Donohue and G. Aranovich, *Adv. Colloid Interface Sci.*, 1998, **76**, 137–152.
33 A. B. McEwen, H. L. Ngo, K. LeCompte and J. L. Goldman, *J. Electrochem. Soc.*, 1999, **146**, 1687–1695.
34 L. Zhang, F. Zhang, X. Yang, K. Leng, Y. Huang and Y. Chen, *Small*, 2013, **9**, 1342–1347.
35 J. Jagiello and J. P. Olivier, *Carbon*, 2013, **55**, 70–80.
36 A. Puziy, O. Poddubnaya, B. Gawdzik and M. Sobiesiak, *Adsorption*, 2016, **22**, 459–464.